

Journal of Materials Chemistry A

Accepted Manuscript



This is an *Accepted Manuscript*, which has been through the Royal Society of Chemistry peer review process and has been accepted for publication.

Accepted Manuscripts are published online shortly after acceptance, before technical editing, formatting and proof reading. Using this free service, authors can make their results available to the community, in citable form, before we publish the edited article. We will replace this *Accepted Manuscript* with the edited and formatted *Advance Article* as soon as it is available.

You can find more information about *Accepted Manuscripts* in the [Information for Authors](#).

Please note that technical editing may introduce minor changes to the text and/or graphics, which may alter content. The journal's standard [Terms & Conditions](#) and the [Ethical guidelines](#) still apply. In no event shall the Royal Society of Chemistry be held responsible for any errors or omissions in this *Accepted Manuscript* or any consequences arising from the use of any information it contains.

Shape- and Morphology-controlled Metal Organic Framework Template for High-Efficiency Solid-state Dye-Sensitized Solar Cells

Cite this: DOI: 10.1039/x0xx00000x

Won Seok Chi[‡], Dong Kyu Roh[‡], Chang Soo Lee,^a Jong Hak Kim^{*a}

Received 00th January 2012,
Accepted 00th January 2012

DOI: 10.1039/x0xx00000x

www.rsc.org/

This report provides a facile process to produce shape- and morphology-controlled MIL-125(Ti), a subclass of metal organic frameworks (MOFs) using poly(ethylene glycol) diglycidyl ether (PEGDGE) as a structure directing agent. Upon deliberate calcination, MIL-125(Ti) is converted to mesoporous hierarchical TiO₂ (hier-TiO₂) with anatase phase, a large surface area and a variety of nanostructures. The morphology changes from 200-nm circular plates to 1- μ m bipyramid with increasing PEGDGE amount, indicating the pivotal role of PEGDGE as a shape controller. When the hier-TiO₂ is deposited onto a nanocrystalline TiO₂ (nc-TiO₂) layer as the scattering layer, the dye-sensitized solar cell (DSSC) with a quasi-solid-state polymer electrolyte records a high conversion efficiency (7.1% at 100 mW/cm²), which is much higher than that of DSSCs with nc-TiO₂ layer only (4.6%) or with a commercial scattering TiO₂ (cs-TiO₂) on a nc-TiO₂ layer (5.0%). A solid-state DSSC using a single component solid polymer, i.e., poly((1-(4-ethenylphenyl)methyl)-3-butyl-imidazolium iodide (PEBII), also exhibits excellent efficiency of up to 8.0%. The improved efficiency results from the pivotal role of the hier-TiO₂ in improving the surface area and light harvesting properties, as demonstrated by N₂ adsorption/desorption isotherm, reflectance spectroscopy, incident photon-to-current efficiency (IPCE), and electrochemical impedance spectroscopy (EIS) analyses.

Introduction

There has been a large focus on dye-sensitized solar cells (DSSCs) as a promising alternative to conventional silicon solar cells because of their high efficiency, low cost, and easy fabrication.¹ Most of the current research has focused on enhancement of device performance, which can be achieved through the development of novel sensitizers,²⁻⁴ metal oxide photoanodes,⁵⁻⁹ catalytic counter electrodes,¹⁰⁻¹³ or electrolytes.¹⁴⁻¹⁶ Among these, the photoanode is an especially important component as it directly affects dye absorption, light trapping ability, charge recombination, and interfacial contact between electrode and electrolyte. Typically, mesoporous TiO₂ is employed as a photoanode material because of its suitable energy level, superior dye absorption ability, and ease of structure control.

As a main element of photoanodes, a nanocrystalline TiO₂ layer is generally deposited on a transparent conducting oxide substrate for dye adsorption. However, this approach has some disadvantages such as low surface area, poor interconnectivity, and smaller light scattering ability because of the poorly organized morphology resulting from small and regular particle size without effective pores. To address these issues, light scattering particles with a large size were deposited onto a nanocrystalline TiO₂ layer to harvest reflecting light.¹⁷⁻²³ This

method increased the light scattering ability as well as the dye loading amount of the photoanode, resulting in enhanced solar energy conversion efficiency in DSSCs.

Despite the high-energy conversion efficiency of DSSCs based on a conventional liquid electrolyte, solid-state or quasi-solid-state DSSCs have recently received great attention because of the need for long-term stability, flexible design, and lightweight cells.²²⁻²⁸ In particular, DSSCs with enhanced energy conversion efficiency and long-term stability need to be developed for future applications such as building integrated photovoltaics. Not only for DSSC, but also for energy storage devices such as rechargeable batteries, the design of solid-state electrolyte is of pivotal importance to obtain durable performance as well as high efficiency.²⁹⁻³¹ One important consideration for such DSSCs is to obtain deep penetration of solid electrolytes with large molecular volume into the TiO₂ mesopores, which is largely affected by the pore size, porosity, and pore interconnectivity. Despite much progress in incorporating solid-state or quasi-solid electrolytes,²²⁻²⁸ there have not been extensive efforts to enhance the device performance by modification of photoanode structures.

Metal organic frameworks (MOFs) have been widely investigated for their attractive unique properties, which can be tuneable by the design of the coordination between metal ions

and organic linkers. MOFs can possess infinite features such as frameworks geometries, pore sizes, and functionalities by tailoring both organic ligand and metal selection. Their highly flexible potential make them candidates for wide applications in the field of gas adsorption separation, catalysts, sensors, and batteries, which are in demand for sustainable and renewable energy devices.³²⁻³⁴

Recently, MOFs have been researched as promising photovoltaic materials in DSSCs. Cu-based MOFs were substituted as a new sensitizer instead of N719 dye using a layer-by-layer technique.³⁵ Mg-MOF was introduced into a polymer composite electrolyte by UV radiation, which increased the photoenergy conversion efficiency through interactions between carboxyl groups in Mg-MOF and hydroxyl groups in the TiO₂ surface layer.³⁶ Furthermore, a metal-organic gel electrolyte composed by coordination of Al³⁺ and 1,3,5-benzenetricarboxylate provided good accommodation ability.³⁷ For electrode application, MOFs worked as both template and precursor to provide functional materials with a high surface area retaining particle morphology. Cobalt sulfide nanoparticles derived from surfactant assisted the preparation of zeolite imidazole framework-67 (ZIF-67) with high surface area and good catalytic properties. As a result, CoS-derived counter electrode-based DSSCs showed a higher solar power conversion efficiency than Pt-based counter electrodes.³⁸ Leaf-like ZIF film was also converted to a porous ZnO nanosheet photoanode, which enabled high dye loading, efficient electrolyte diffusion, rapid dye adsorption by nanopores, and good light harvesting ability.³⁹ Also, hierarchical ZnO parallelepipedes were prepared from MOF-5, a subclass of MOF series, and used as a scattering layer in the DSSCs.⁴⁰ However, most previous studies are based on a ZnO photoanode with which it is difficult to achieve a high efficiency because of the low surface area and dye loading.

In this study, we report a facile way of preparing multifunctional, hierarchical, anatase TiO₂ with large surface area and various morphologies directly derived from MIL-125(Ti), a subclass of MOF series. In particular, poly(ethylene glycol) diglycidyl ether (PEGDGE) was employed as a structure-directing agent to form various MIL-125(Ti) structures. Upon deliberate calcination, MIL-125(Ti) was converted to hierarchical TiO₂ (hier-TiO₂) with a large surface area and a variety of nanostructures. The hier-TiO₂ synthesized was used to form top scattering layers on a nanocrystalline TiO₂ (nc-TiO₂) layer for use in DSSC applications, and these hier-TiO₂ layers were characterized by scanning electron microscopy (SEM), transmission electron microscopy (TEM), X-ray diffraction (XRD), N₂ adsorption-desorption isotherm analysis, UV-visible light absorption, and reflectance spectroscopy. The performance of DSSCs was investigated by measuring current density-voltage (J-V) curves, incident photon-to-current efficiency (IPCE), and electrochemical impedance spectroscopy (EIS).

Experimental section

Materials

Titanium (IV) butoxide (TBT), terephthalic acid (4-benzenedicarboxylate, BDC), poly(ethylene glycol) diglycidyl ether (PEGDGE), poly(ethylene glycol) (PEG10k, 10,000 g/mol), lithium iodide (LiI), 1-methyl-3-propylimidazolium iodide (MPII), iodine (I₂), dimethylformamide (DMF), methanol, ethanol, and acetonitrile were purchased from Aldrich and used without further purification. Ruthenium dye (535-bisTBA, N719) was purchased from Solaronix, and commercially available TiO₂ paste (Dyesol paste, 18NR-T) was purchased from Dyesol. FTO conductive glass was purchased from Pilkington, France.

Preparation of MIL-125(Ti)

First, 3.5 g of terephthalic acid was completely dissolved in DMF solvent. Different amounts (0, 0.06, 0.6, and 1.2 ml) of PEGDGE, 1.82 ml of titanium butoxide, and 7 ml of methanol were sequentially added to this solution, followed by stirring for 20-30 min to produce homogeneous mixtures. The resultant solutions were hydrothermally reacted in an autoclave at 150°C for 24 h. The synthesized MIL-125(Ti) was centrifuged at 10,000 rpm for 30 min and washed with fresh methanol several times. The final products were dried in a vacuum oven overnight at 50°C to completely evaporate the DMF. MIL-125(Ti) synthesized using 0, 0.06, 0.6, and 1.2 ml of PEGDGE was named MIL-125(Ti)1, MIL-125(Ti)2, MIL-125(Ti)3, and MIL-125(Ti)4, respectively.

Conversion of MIL-125(Ti) to hierarchical TiO₂ (hier-TiO₂)

The synthesized MIL-125(Ti) was calcined at 380°C for a long time (i.e., 5 h) with a slow increase in temperature (i.e., 10°C/min) to produce a mesoporous anatase structure while controlling the release of gas from the MIL framework.⁴¹ Setting temperature moderate was the most important to generate a highly mesoporous structure, while maintaining the basic framework of MIL-125(Ti) without pore blocking and formation of big pores by the connection of small pores.

Preparation of photoanodes

As-prepared hier-TiO₂ particles (0.1 g) were dispersed in 1 ml absolute ethanol solvent by sonication and stirring for 5 h. After distribution of particles in solution, 0.4 ml of α -terpinol and 0.05 g of ethyl cellulose were added to the suspension solutions to increase the viscosity. The resultant solutions were sonicated for 30 min and stirred overnight for perfect dissolution of organic materials in the TiO₂ suspension. Ethanol solvents were evaporated during stirring while maintaining a homogeneous state, resulting in the formation of highly viscous TiO₂ paste. As-prepared TiO₂ pastes were doctor-bladed onto the nc-TiO₂ layer and heated in a drying oven at 50°C for 1 h and 80°C for 1 h. This process was performed to prevent crack formation after calcination. Finally, the TiO₂ photoanodes were calcinated at 500°C for 30 min. TiCl₄ post-treatment was not necessary because of the good physical and adhesion properties.

Fabrication of DSSCs

DSSCs with active area of 0.16 cm^2 were fabricated according to our previous studies.⁴²⁻⁴⁵ First, the FTO (Pilkington Co. Ltd., 8Ω) glass pieces were cut ($1.5 \text{ cm} \times 2 \text{ cm}$) and cleaned with acetone and ethanol under sonication. For the blocking layer, Ti(IV) bis(ethyl acetoacetato) diisopropoxide solution in 1-butanol was spin-coated onto FTO glass and then the glass was heated stepwise to 450°C and maintained at this temperature for 30 min. A 6- to $7\text{-}\mu\text{m}$ thick n- TiO_2 layer was prepared on the blocking layer on FTO substrate using commercial TiO_2 paste (Dyesol paste, 18NR-T) by the doctor-blade method and then calcinated at 450°C for 30 min, resulting in the formation of a transparent TiO_2 photoanode. The TiO_2 photoanodes were immersed in dye solution containing 13 mg N719 in 50 ml absolute ethanol solution and incubated in an oven at 50°C for 3 h. The resulting photoanodes were washed with pure ethanol several times and dried by air gun. The Pt counter electrode was prepared by spin-coating solution containing 7 mM $\text{H}_2\text{PtCl}_6 \cdot \text{H}_2\text{O}$ in 2-propanol onto the FTO glass, followed by heat treatment at 450°C for 30 min. The quasi-solid-state electrolyte was prepared using PEG10k ($M_n = 10,000 \text{ g/mol}$), MPII, LiI and I_2 in acetonitrile solvent. Poly((1-(4-ethenylphenyl)methyl)-3-butyl-imidazolium iodide) (PEBII) without any additives was used as the single component solid electrolyte. The prepared electrolytes were directly cast onto the photoanode. Both electrodes were superimposed and pressed between two glass plates to slowly evaporate the solvent and produce a thin electrolyte layer. The cells were placed in a vacuum oven for 1 day to allow complete evaporation of the solvent and then sealed with an epoxy resin.

The photovoltaic properties of DSSCs were characterized using a Keithley Model 2400 and a 1000 W xenon lamp (Oriel, 91193). The light intensity was homogeneous over a $20 \times 20 \text{ cm}^2$ area. The mismatch between the simulated light and natural sunlight was calibrated by adjusting the photocurrent density of a Si solar cell (Fraunhofer Institute for Solar Energy System, Mono-Si + KG filter, Certificate No. C-ISE269) for a sunlight intensity of unity (100 mW/cm^2). More than three identical DSSCs were fabricated and tested to increase the reliability of the characterizations, and all of the DSSCs were characterized at room temperature using a thermoelectric cooler to maintain the temperature. EIS data were measured using an electrochemical workstation (Keithley Model 2400) with a frequency range from 0.01 Hz to 0.1 MHz and AC amplitude of 0.2 V.

Measurement of dye loading

N719 dye-sensitized TiO_2 photoanodes with an active area of 1.0 cm^2 were immersed in 10.0 ml of 0.1 M NaOH in a 1:1 (by volume) mixed solvent of ethanol and deionized water. The resulting solutions were stirred until the N719 dye molecules detached fully from the surface of the TiO_2 photoanodes. Finally, the original N719 dye loading on the photoanodes was calculated based on UV-visible spectroscopy analysis of the solutions using the absorbance peak

value at 515 nm according to the Beer–Lambert law ($A = \epsilon lc$), where A is the absorbance at 515 nm, $\epsilon = 14,100 \text{ M}^{-1} \text{ cm}^{-1}$ is the molar extinction coefficient of the N719 dye at 515 nm, l is the length of the analytical light path, and c is the concentration of the N719 dye.

Characterization

Materials synthesis was characterized by Excalibur Series FT-IR (DIGLAB Co.) instrument over a frequency range of $4,000\text{--}400 \text{ cm}^{-1}$. Each element was investigated by XPS equipped with a K-alpha (Thermo, UK) with a monochromated Al $K\alpha$ X-ray source. UV-vis spectroscopy was performed with a spectrophotometer (Shimadzu) in the range of $300\text{--}800 \text{ nm}$. The thermal stability of materials was determined by TGA (Mettler Toledo TGA/SDTA 851e, Columbus, OH) under air atmosphere from 50°C to 700°C at a rate of 20°C/min . The morphology of materials was characterized by energy-filtering transmission electron microscopy (EF-TEM, Carl Zeiss, LIBRA 120, Germany).

Results and Discussion

Hydrothermal reaction of the solution containing TBT, BDC, and PEGDGE was conducted at 150°C for 24 h to synthesize MIL-125(Ti) with various structures and sizes. To confirm successful preparation of MIL-125(Ti), the FT-IR spectra were measured as shown in **Figure 1a**. The strong absorption band at 1381 cm^{-1} and weak absorption band at 1437 cm^{-1} corresponded to carbonyl symmetric stretching vibrations. Also, three absorption bands from 1400 to 1500 cm^{-1} are assigned to carbonyl asymmetric stretching vibration modes. The small shoulder peak at 1255 cm^{-1} indicates the C–H symmetric stretching vibrations of the benzene ring. The sharp peaks presented in the region of $400\text{--}800 \text{ cm}^{-1}$ correspond to Ti–O–Ti–O vibrations. The intensity of the carboxylic acid functional group of MIL-125(Ti) in the range of $1300\text{--}700 \text{ cm}^{-1}$ gradually increased with increasing amount of PEGDGE in the reaction solution, indicating surface modification of MIL-125(Ti) by PEGDGE.

TGA is a useful tool that can be used to confirm the transition process from MIL-125(Ti) to TiO_2 . As shown in **Figure 1b**, the first weight loss was observed under the calcination process up to 100°C , and is due to residual solvents that were primarily water adsorbed onto MIL-125(Ti). In the range of $100\text{--}300^\circ\text{C}$, the second slow weight loss was caused by removal of DMF molecules and unreacted organic chemicals captured within MIL-125(Ti) pores. Above 300°C the stable MIL-125(Ti) started to undergo phase transition and structural reorganization to TiO_2 without external configuration of particles, probably due to the loss of hydroxo groups.⁴⁶ It was confirmed that MIL-125(Ti) instantaneously decomposed to TiO_2 at 450°C and maintained the resultant TiO_2 structure under further heat treatment.

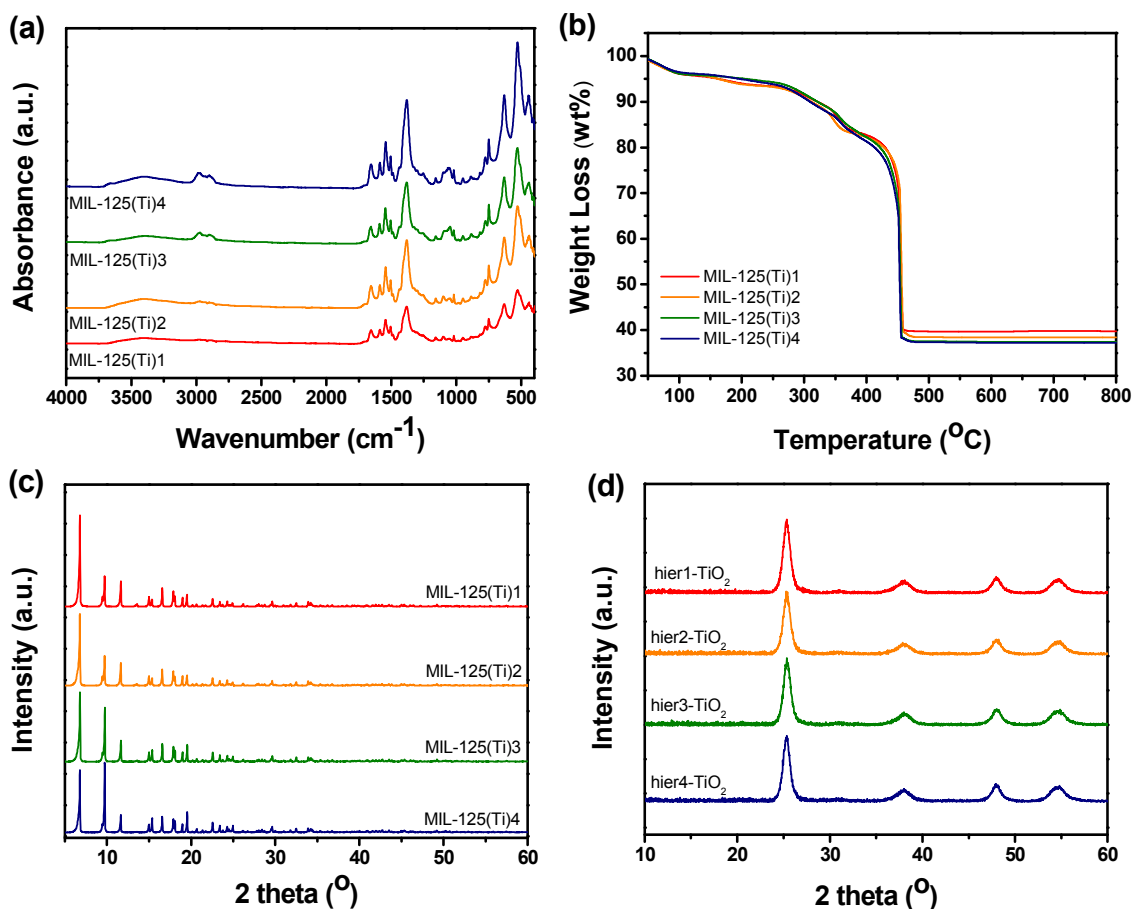


Fig. 1 (a) FT-IR spectra, (b) TGA curves of MIL-125(Ti) particles, (c) XRD patterns of MIL-125(Ti) and (d) XRD patterns of hier-TiO₂ particles.

XRD patterns of MIL-125(Ti) series produced by different amounts of PEGDGE were measured to identify the crystal phase of materials, as shown in **Figure 1c**. The crystal structure was composed of μ -OH corner-sharing TiO₆ octahedra chains through Ti⁴⁺ ions, which were interconnected by BDC molecules to develop three-dimensional architecture pores.⁴⁷ The crystal structure and phases of MIL-125(Ti) series were consistent with previously reported values.⁴⁶⁻⁴⁸ However, the relative peak intensity was primarily affected by the amount of PEGDGE used for hydrothermal process. With increasing amount of PEGDGE, the peaks at diffraction angles (2θ) of 9.7°, 15.3°, 19.5°, and 25.0° increased whereas the peaks at 6.7°, 11.6°, 15.0°, 16.5°, and 17.9° decreased. This indicates that the growth of MIL-125(Ti) crystalline structure was affected by PEGDGE and thus the crystal was reconstructed, leading to a change in particle morphology and surface area.⁴⁹ After calcination, the pure anatase TiO₂ phase structure was observed for all MIL-125(Ti)-based hierarchical TiO₂ (denoted as hier-TiO₂)

regardless of the PEGDGE content, as shown in **Figure 1d**. The peaks at 25.3°, 37.9°, 47.8°, and 54.7° corresponded to reflections from the (101), (004), (200), and (105) crystal planes of anatase TiO₂, respectively.

The MIL-125(Ti) series, controlled by the amount of PEGDGE in the synthesis procedure, presented various particle sizes (200 nm–1 μ m) and shapes (circular plate to truncated bipyramids), as seen in **Figure 2a-d**. Hydrothermal reaction of a homogenous solution composed of TBP and BDC in DMF/methanol mixture without PEGDGE produced a small particle size (200 nm) and circular plate morphology. Use of the modulator PEGDGE resulted in more phase separation between solvent and precursor, leading to an aggregated structure and larger particle size up to 1 μ m. Furthermore, the direction perpendicular to the circular plate generated new growth and facet formation that was exposed on the crystal structure, triggering formation of truncated bipyramids.⁵⁰

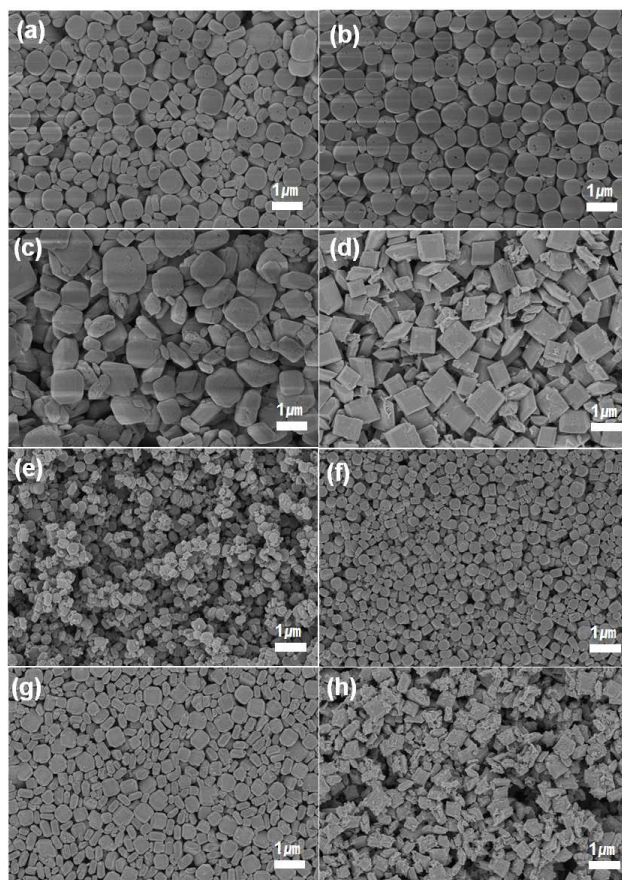


Fig. 2 SEM images of (a) MIL-125(Ti)1, (b) MIL-125(Ti)2, (c) MIL-125(Ti)3, (d) MIL-125(Ti)4, (e) hier1-TiO₂, (f) hier2-TiO₂, (g) hier3-TiO₂, and (h) hier4-TiO₂.

Figure 2e-h shows the SEM images of mesoporous anatase hier-TiO₂ particles derived from MIL-125(Ti) *via* dispersion in ethanol solution and casting onto glass substrate. Distributed hier-TiO₂ particles were densely packed and maintained their morphology, even after calcination with crystal structure alternation. Only TiO₂ particle sizes were reduced by shrinkage of MIL-125(Ti), in which the pores were formed from frameworks of intertwined Ti metal and organic linker after calcination. These submicro and microsized hier-TiO₂ particles are expected to efficiently enhance the light scattering ability.

To more clearly identify the morphology and size of MIL-125(Ti) and hier-TiO₂ particles, TEM observations were conducted as shown in **Figure 3**. MIL-125(Ti) exhibited a large size of greater than 500 nm without evident pore structure due to the very small pore size of less than 2 nm. The framework structure gradually changed from circular plates to truncated bipyramids, consistent with the above SEM observations. Upon calcination, well-defined TiO₂ particles were generated with organized mesopores and large surface area, which would be effective for enhancing dye loading and pore filling of the polymer electrolyte. All hier-TiO₂ particles retained

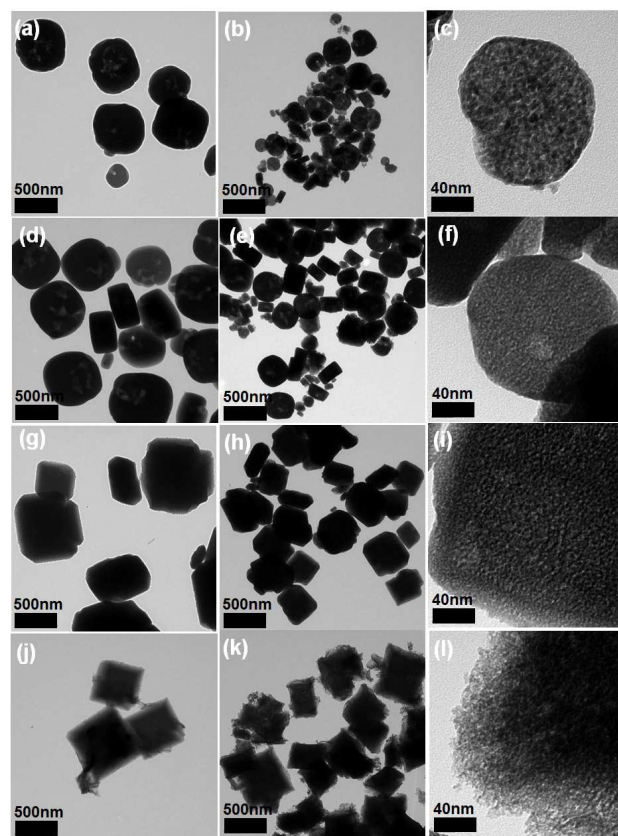


Fig. 3 TEM images of (a) MIL-125(Ti)1, (b,c) hier1-TiO₂, (d) MIL-125(Ti)2, (e,f) hier2-TiO₂, (g) MIL-125(Ti)3, (h,i) hier3-TiO₂, (j) MIL-125(Ti)4, and (k,l) hier4-TiO₂.

highly interconnected pores with shrunken particle sizes. These special characteristics of mesoporous anatase TiO₂ would act to booster solar energy performance, which needs a large surface area and excellent light scattering properties.

Under the mild calcination conditions, MIL-125(Ti) series were completely converted to anatase mesoporous hier-TiO₂ particles. The specific surface area of MIL-125(Ti) and hier-TiO₂ particles is summarized in **Table S1**, as determined by N₂ adsorption-desorption measurements using the BET method. Because of the small-scale frameworks coordinating the organic linker and metal ions, the MIL-125(Ti) series exhibited a high surface area of over 1300 m²/g, which is comparable to recently reported values.⁴⁸⁻⁵⁰ After calcination, the pores of MIL-125(Ti) were shrunken, such that anatase TiO₂ particles had an area of over 100 m²/g, but retained the particle frameworks. As shown in **Figure 4a**, Type-IV isotherms with H1-type hysteresis loops at P/P₀ = 0.5–0.8 were observed for all hier-TiO₂ particles, indicating the presence of large mesopores. The average pore diameters of hier-TiO₂ particles were quite similar at approximately 6–10 nm, as estimated using the BJH method (**Figure 4b**).

UV-visible absorption spectra were measured to investigate changes in dye loading of bilayer photoanodes of hier-TiO₂ on nc-TiO₂. The results are summarized in **Table 1**. The hier-TiO₂ layered photoanodes exhibited greater dye loading than neat nc-TiO₂ monolayered photoanode due to the increased film thickness and increased surface area. In particular, the deposition of hier-TiO₂ layer on nc-TiO₂ photoanodes resulted in a nearly two-fold increase in dye loading (from 77 to 139 nmol/cm²), which would help to significantly improve the efficiency of the DSSCs.

Figure 4c shows photographs of different hier-TiO₂/nc-TiO₂ bilayer photoanodes and neat nc-TiO₂ monolayer photoanode. By the naked eye it was obvious that the photoanodes became opaque after the deposition of hier-TiO₂ on transparent nc-TiO₂, demonstrating efficient light reflectance and scattering. The reflective abilities of hier-TiO₂/nc-TiO₂ bilayers and neat transparent nc-TiO₂ monolayer were measured by UV-vis reflectance spectroscopy in the visible range from 300–800 nm as shown in **Figure 5a**. The photoanode with a transparent nc-TiO₂ monolayer presented low reflective ability with retaining values between 10% and 20% and maximum reflectance at 390 nm. On the other hand, higher reflective properties were observed for the bilayer

photoanodes composed of scattering hier-TiO₂ on nc-TiO₂ layer over the entire range, recording over 50% reflectance. All of the photoanodes with a scattering layer exhibited similar reflectance ability without large differences. This reflectance ability could strongly affect the performance of the DSSCs, which might be dependent on light trapping ability of the photoanode for recycling light.

Surface and cross-sectional SEM images of the photoanodes layered by the doctor blading technique are shown in **Figure S1 and S2**. The surface SEM images of hier-TiO₂ on nc-TiO₂ photoanodes were not significantly different from those of neat hier-TiO₂ particles (**Figure 2e-h**), indicating that the original morphology and particle size were not perturbed by the organic binder (i.e., ethyl cellulose and α -terpinol) and the doctor blading technique. However, the interconnectivity between the TiO₂ particles could be enhanced to provide increased electron transportation. The dual porous structure of the hier-TiO₂ layer formed by small inner pores in the particles as well as large pores between the particles would be effective in improving energy conversion efficiency based on a multifunctional effect. In general, commercial scattering layers are deposited with less than 4 μ m thickness because of their own resistance and lower

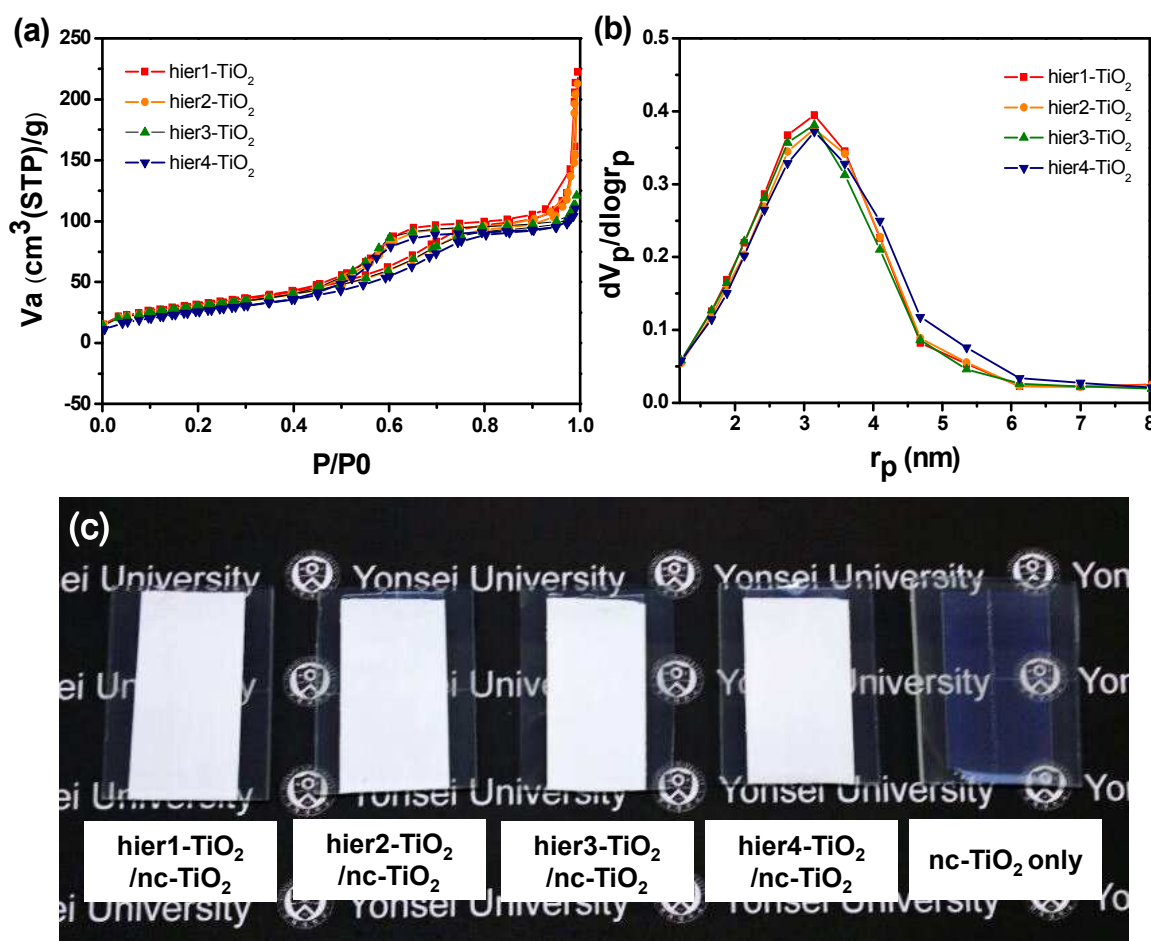


Fig. 4 (a) N₂ adsorption-desorption isotherms and (b) pore size distribution of hier-TiO₂ particles determined by the BJH method, (c) photographs of hier-TiO₂/nc-TiO₂ bilayer and nc-TiO₂ monolayer photoanodes.

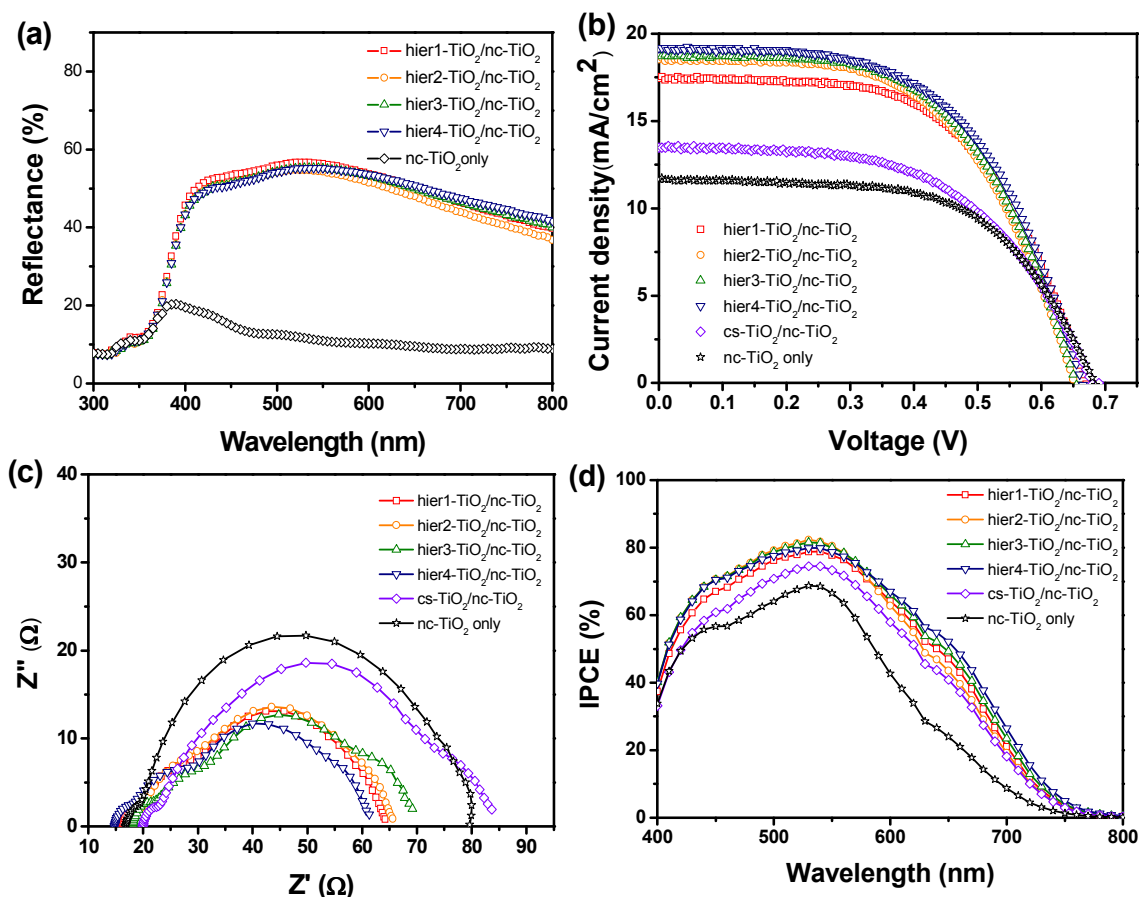


Fig. 5 (a) UV-visible reflectance spectra of hier-TiO₂/nc-TiO₂ bilayer and nc-TiO₂ monolayer photoanodes, (b) J-V curves, (c) Nyquist plots, and (d) IPCE curves of DSSCs fabricated with a quasi-solid-state polymer electrolyte and the different photoanodes under one sun illumination conditions (100 mW/cm²).

effectiveness of pore filling.¹⁷⁻²³ However, we were able to increase the thickness of the hier-TiO₂ layer up to approximately 6 μm by controlling the viscosity of the paste and using the doctor blading technique, resulting in improved DSSC efficiency. This is because the hier-TiO₂ scattering layer has a greater ability to improve dye adsorption and light utilization, without having any negative effect on the pore filling of polymer electrolyte even at higher film thickness.

The solid-state or quasi-solid-state DSSCs are more advantageous than the liquid electrolyte-based counterpart because of the need for long-term stability, a flexible design, and light-weight cells. DSSCs based on a hier-TiO₂ layer were fabricated using a quasi-solid-state polymer electrolyte consisting of PEG10K, MPII, LiI, and I₂. This quasi-solid-state polymer electrolyte is based on the ethylene oxide group and a high molecular weight (10,000 g/mol) enough to produce better mechanical stability and faster ion transportation via the Grotthuss hopping compared to the ones reported by other groups.⁵¹⁻⁵³ The J-V curves of the DSSCs with different photoanode structures were measured at 100 mW/cm² as shown in **Figure 5b** and their photovoltaic parameters, including short-circuit current density (J_{sc}), open-circuit voltage (V_{oc}), fill

factor (FF), and overall energy conversion efficiency (η), are summarized in **Table 1**. The hier-TiO₂ bilayer photoanodes enhanced the solar energy conversion efficiency to as high as 7.1%, which is much higher than that of the nc-TiO₂ monolayer photoanode (4.6%). The obtained cell efficiency was not significantly changed at room temperature up to several days. There were no significant differences in FF and V_{oc} values among the DSSCs. Thus, the much higher efficiency of hier-TiO₂ based DSSCs is mostly attributed to an improvement in the J_{sc} value, resulting from increased dye loading and light scattering effect. Although there was a slight difference among the hier-TiO₂ based DSSCs, hier4-TiO₂ showed the highest efficiency, which will be characterized in next section using EIS and IPCE measurements.

The electrochemical analysis provides important information on the internal and interfacial resistances in equivalent circuits. The EIS spectra of DSSCs fabricated with hier-TiO₂ based photoanodes are shown in **Figure 5c** and summarized in **Table 1**. The resistance parameters consisted of Ohmic series resistance of conducting glass substrate (R_s), interfacial charge transfer resistance between counter electrode and electrolyte (R_1), interfacial charge transfer resistance between the photoanode and electrolyte (R_2), and mass transport

Table 1. Photovoltaic parameters of the DSSCs fabricated with a quasi-solid-state polymer electrolyte and the different photoanodes under one sun illumination condition (at 100 mW/cm²).

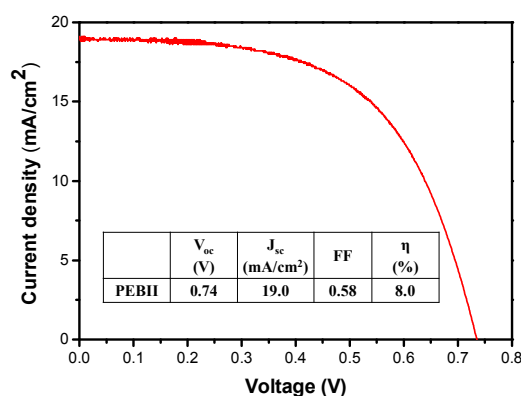
| Photoanode | Dye loading (nmol cm ⁻²) | V _{oc} (V) | J _{sc} ^a (mA cm ⁻²) | FF | η (%) | R _s (Ω) | R ₁ (Ω) | R ₂ (Ω) | W _s (Ω) |
|---|--------------------------------------|---------------------|---|------|-------|--------------------|--------------------|--------------------|--------------------|
| hier1-TiO ₂ /nc-TiO ₂ | 139 | 0.66 | 17.4(18.6) | 0.56 | 6.6 | 16.1 | 2.9 | 38.0 | 7.0 |
| hier2-TiO ₂ /nc-TiO ₂ | 137 | 0.65 | 18.5(18.8) | 0.55 | 6.7 | 17.0 | 2.5 | 38.5 | 7.5 |
| hier3-TiO ₂ /nc-TiO ₂ | 128 | 0.65 | 18.7(19.5) | 0.55 | 6.8 | 18.1 | 3.3 | 37.3 | 10.5 |
| hier4-TiO ₂ /nc-TiO ₂ | 113 | 0.66 | 19.1(19.7) | 0.55 | 7.1 | 14.8 | 3.0 | 37.2 | 6.3 |
| cs-TiO ₂ /nc-TiO ₂ | - | 0.68 | 13.5(16.9) | 0.54 | 5.0 | 19.9 | 3.0 | 50.1 | 10.7 |
| nc-TiO ₂ only | 77 | 0.68 | 11.7(14.6) | 0.57 | 4.6 | 16.7 | 2.4 | 53.9 | 7.0 |

^a Values in parentheses refer to the J_{sc} obtained from IPCE curves

resistance related to electrolyte redox couple (I⁺/I₃⁻), which is known as Warburg diffusion (W_s). The R_s and R₁ values of the DSSCs were not significantly different because these parameters were not strongly related to resistance of the photoanode element. The R₂ value is a pivotal parameter for investigating the charge transfer corresponding to the photoanode, which determines how effectively the TiO₂ scattering layer functions electrochemically. The R₂ values of DSSCs with hier-TiO₂/nc-TiO₂ bilayer photoanodes (37.2 ~ 38.5 Ω) were much smaller than that of nc-TiO₂ monolayer (53.9 Ω) or cs-TiO₂/nc-TiO₂ double layer photoanode (50.1 Ω). In particular, the R₂ value of hier4-TiO₂ based DSSC was the smallest, indicating smaller charge transfer resistance at the photoanode interface. The hierarchical structure with high porosity and good connectivity based on both inner mesopore and inter spaces of hier-TiO₂ facilitated deep penetration of polymer electrolyte and improved conductivity, leading to efficient ion transportation and dye regeneration.

IPCE is defined as the ratio of the number of electrons in the external circuit produced by incident photons to the number of generated charge carriers at a given wavelength. Hence, the light scattering effect can be evaluated by measuring the IPCE spectra of DSSCs. The IPCE spectrum is directly related to the J_{sc} value measured in J-V curves, which is largely determined by dye loading, electron transport, and light harvesting. The IPCE spectra of DSSCs with a quasi-solid-state polymer electrolyte and various photoanodes were measured at 100 mW/cm² as a function of the illumination wavelength, as shown in **Figure 5d**. To ensure size dependency as well as dye loading ability, the normalized IPCE curves were also plotted by dividing entire IPCE values by the highest IPCE value to give a maximum IPCE value of 1 (**Figure S3**). The IPCE values of the DSSCs fabricated with hier-TiO₂/nc-TiO₂ bilayer photoanodes were always much higher than those of nc-TiO₂ monolayer or the cs-TiO₂/nc-TiO₂ double layer over the whole spectral range. This indicates that DSSCs based on hier-TiO₂ photoanodes exhibited enhanced light utilization ability through light scattering layer deposition. The maximum IPCE value was observed at 525 nm, corresponding to the absorption peak of N719 dye, due to visible t₂ to π* metal to ligand charge transfer. The IPCE value is a result of the amount of dye absorption at lower wavelengths below 525 nm, but is related to light scattering efficiency at wavelengths above 525 nm. The DSSCs with bilayer photoanodes exhibited higher IPCE values compared to those with a neat nc-TiO₂ layer-based photoanode at both low (< 525 nm) and high (> 525 nm) wavelengths, which is indicative of enhancement of both dye loading

and light scattering properties. The light scattering effect increased with an increase in TiO₂ particle size, consistent with the reflectance results in the wavelength range between 600 and 700 nm. Despite lower dye loading, the hier4-TiO₂ based DSSC showed the highest efficiency as a result of better light scattering properties at higher wavelength regions, indicating that light scattering is more important than dye loading for the scattering layer.

**Fig. 6** J-V curve of the solid-state DSSC fabricated with hier4-TiO₂/nc-TiO₂ photoanode and a solid PEBII electrolyte at 100 mW/cm².

We also tested the effectiveness of hier-TiO₂ as a light scattering layer by fabricating solid-state DSSCs employing a single component solid PEBII electrolyte, as shown in **Figure 6**. PEBII solidifies as a result of free radical polymerization of an ionic liquid, and the ionic conductivity reached 2.0×10^{-4} S cm⁻¹ at room temperature due to the well-organized structure coupled with the π-π stacking interactions. Thus, PEBII functioned well as the solid electrolyte even without any additives such as iodide salt or iodine (I₂).⁴²⁻⁴⁵ The efficiency of solid-state DSSCs based on a hier-TiO₂/nc-TiO₂ double layer reached 8.0%, which is among the highest values reported for N719-based solid-state DSSCs.^{42-45,54-60} This again demonstrated that the hier-TiO₂ layer is highly efficient because of its multifunctionality; namely, (1) a large surface area that allows high levels of dye loading and thereby enhances the light harvesting efficiency, (2) a morphology that reflects the light back

into the nc-TiO₂ layer, and (3) higher porosity that allows deep penetration of large molecular volume polymer electrolyte.

Conclusion

We have reported a synthesis of anatase hier-TiO₂ nanostructures derived from shape- and morphology-controlled MIL-125(Ti) via direct conversion by a calcination process. MIL-125(Ti) functioned as both template and precursor with control of structure and particle size through the use of PEGDGE as the structure-directing agent in the hydrothermal reaction. Use of large amounts of PEGDGE produced a larger particle size and changed the morphology from a circular plate to bipyramid. The hier-TiO₂ possessed high porosity as well as good interconnectivity, making it effective as the scattering layer in a bilayer photoanode for DSSC. The DSSC fabricated with hier-TiO₂/nc-TiO₂ bilayer photoanode and a quasi-solid-state polymer electrolyte exhibited greatly improved solar cell performance efficiency as high as 7.1%, compared to that of the nc-TiO₂ monolayer photoanode based DSSC (4.6%). The efficiency of solid-state DSSCs fabricated using a single component PEBII solid polymer also reached a high value of 8.0%, which is among the highest values reported for N719-based solid-state DSSCs. The improved light harvesting efficiency of cells including hier-TiO₂ layers was attributed to their bifunctionality, namely their ability to reflect light back into the dye as well as their high surface area that allowed high dye loading. This MOF template strategy demonstrated the possibility of introducing MOFs into photovoltaic energy device application and provided a significant contribution to the development of high-performance DSSCs, including structure controllable MOF materials. Furthermore, this strategy is very versatile and can be applied to other types of photovoltaics such as perovskite solar cells to obtain better performance with scattering effect as well as high absorption ability.

Acknowledgements

This work was supported by the Center for Advanced Meta-Materials (NRF-2014M3A6B3063716), the Korea Center for Artificial Photosynthesis (NRF-2009-0093883), and the Human Resources Program in Energy Technology of the Korea Institute of Energy Technology Evaluation and Planning (KETEP, 20154010200810).

Notes and references

Department of Chemical and Biomolecular Engineering, Yonsei University, 50 Yonsei-ro, Seodaemun-gu, Seoul 120-749, South Korea. Fax: +82-2-312-6401; Tel: +82-2-2123-5757; E-mail : jonghak@yonsei.ac.kr

† Electronic Supplementary Information (ESI) available: [details of any supplementary information available should be included here]. See DOI: 10.1039/b000000x/

‡ These authors contributed equally to this work.

- 1 B. O'Regan and M. Gratzel, *Nature*, 1991, **353**, 737-740.
- 2 M. Liu, M.B. Johnston, H.J. Snaith, *Nature*, 2013, **501**, 395-398.
- 3 A. Yella, H.-W. Lee, H.N. Tsao, C. Yi, A.K. Chandiran, M.K. Nazeeruddin, E.W.-G. Diao, C.-Y. Yeh, S.M. Zakeeruddin, M. Grätzel, *Science*, 2011, **334**, 629-634.
- 4 Y.-L. Lee, Y.-S. Lo, *Adv. Funct. Mater.*, 2009, **19**, 604-609.
- 5 S.H. Ahn, D.J. Kim, W.S. Chi, J.H. Kim, *Adv. Mater.*, 2013, **25**, 4893-4897.
- 6 D.K. Roh, W.S. Chi, H. Jeon, S.J. Kim, J.H. Kim, *ChemSusChem*, 2013, **6**, 1384-1391.
- 7 S.H. Ko, D. Lee, H.W. Kang, K.H. Nam, J.Y. Yeo, S.J. Hong, C.P. Grigoropoulos, H.J. Sung, *Nano Lett.*, 2011, **11**, 666-671.
- 8 S. Gubbala, H.B. Russell, H. Shah, B. Deb, J. Jasinski, H. Rypkema, M.K. Sunkara, *Energy Environ. Sci.*, 2009, **2**, 1302-1309.
- 9 X. Tao, P. Ruan, X. Zhang, H. Sun, X. Zhou, *Nanoscale*, 2015, **7**, 3539-3547.
- 10 Y. Xue, J. Liu, H. Chen, R. Wang, D. Li, J. Qu, L. Dai, *Angew. Chem. Int. Ed.*, 2012, **51**, 12124-12127.
- 11 G. Calogero, P. Calandra, A. Irrera, A. Sinopoli, I. Citro, G. Di Marco, *Energy Environ. Sci.*, 2011, **4**, 1838-1844.
- 12 S. Jiang, X. Yin, J. Zhang, X. Zhu, J. Li, M. He, *Nanoscale*, 2015, **7**, 10459-10464.
- 13 H. Wang, K. Sun, F. Tao, D.J. Stacchiola, Y.H. Hu, *Angew. Chem.*, 2013, **125**, 9380-9384.
- 14 F. Bella, A. Sacco, G. Massaglia, A. Chiodoni, C.F. Pirri, M. Quaglio, *Nanoscale*, 2015, **7**, 10459-10464.
- 15 J.K. Koh, J. Kim, B. Kim, J.H. Kim, E. Kim, *Adv. Mater.*, 2011, **23**, 1641-1646.
- 16 W.S. Chi, J.K. Koh, S.H. Ahn, J.-S. Shin, H. Ahn, D.Y. Ryu, J.H. Kim, *Electrochem. Commun.*, 2011, **13**, 1349-1352.
- 17 M. Guo, K. Xie, X. Liu, Y. Wang, L. Zhou, H. Huang, *Nanoscale*, 2014, **6**, 13060-13067.
- 18 Y.-Z. Zheng, X. Tao, L.-X. Wang, H. Xu, Q. Hou, W.-L. Zhou, J.-F. Chen, *Chem. Mater.*, 2010, **22**, 928-934.
- 19 K. Zhu, N.R. Neale, A. Miedaner, A.J. Frank, *Nano Lett.*, 2007, **7**, 69-74.
- 20 Y. Qiu, W. Chen, S. Yang, *Angew. Chem.*, 2010, **122**, 3757-3761.
- 21 H.J. Koo, Y.J. Kim, Y.H. Lee, W.I. Lee, K. Kim, N.G. Park, *Adv. Mater.*, 2008, **20**, 195-199.
- 22 C.S. Lee, J.K. Kim, J.Y. Lim, J.H. Kim, *ACS Appl. Mater. Interfaces*, 2014, **6**, 20842-20850.
- 23 J.A. Seo, D.K. Roh, J.K. Koh, S.J. Kim, B. Jung, J.H. Kim, *Electrochim. Acta*, 2012, **80**, 27-33.
- 24 X. Chen, Q. Tang, B. He, H. Chen, *RSC Adv.*, 2015, **5**, 43402-43407.
- 25 S.H. Ahn, D.J. Kim, W.S. Chi, J.H. Kim, *J. Mater. Chem. A*, 2015, **3**, 10439-10447.
- 26 Y. Duan, Q. Tang, Y. Chen, Z. Zhao, Y. Lv, M. Hou, P. Yang, B. He, L. Yu, *J. Mater. Chem. A*, 2015, **3**, 5368-5374.
- 27 R. D. Costa, F. Werner, X. Wang, P. Grönninger, S. Feihl, F. T. U. Kohler, P. Wasserscheid, S. Hibler, R. Beranek, K. Meyer, D. M. Guldi, *Adv. Energy Mater.* 2013, **3**, 657-665.
- 28 W. Cho, Y.R. Kim, D. Song, H.W. Choi, Y.S. Kang, *J. Mater. Chem. A*, 2015, **3**, 6685-6685.
- 29 J.R. Nair, L. Porcarelli, F. Bella, C. Gerbaldi, *ACS Appl. Mater. Interfaces*, 2015, **7**, 12961-12971.
- 30 W. Guo, X. Xue, S. Wang, C. Lin, Z.L. Wang, *Nano Lett.*, 2012, **12**, 2520-2523.
- 31 V. Chakrapani, F. Rusli, M.A. Filler, P.A. Kohl, *J. Power Sources*, 2012, **216**, 84-88.
- 32 J.-R. Li, R.J. Kuppler, H.-C. Zhou, *Chem. Soc. Rev.*, 2009, **38**, 1477-1504.

- 33 B. Li, Y. Zhang, D. Ma, L. Li, G. Li, G. Li, Z. Shi, S. Feng, *Chem. Commun.*, 2012, **48**, 6151-6153.
- 34 D. Ma, B. Li, X. Zhou, Q. Zhou, K. Liu, G. Zeng, G. Li, Z. Shi, S. Feng, *Chem. Commun.*, 2013, **49**, 8964-8966.
- 35 D.Y. Lee, C.Y. Shin, S.J. Yoon, H.Y. Lee, W. Lee, N.K. Shrestha, J.K. Lee, S.-H. Han, *Sci. Rep.*, 2014, **4**, 3930.
- 36 F. Bella, R. Bongiovanni, R.S. Kumar, M.A. Kulandainathan, A.M. Stephan, *J. Mater. Chem. A*, 2013, **1**, 9033-9036.
- 37 J. Fan, L. Li, H.-S. Rao, Q.-L. Yang, J. Zhang, H.-Y. Chen, L. Chen, D.-B. Kuang, C.-Y. Su, *J. Mater. Chem. A*, 2014, **2**, 15406-15413.
- 38 S.-H. Hsu, C.-T. Li, H.-T. Chien, R.R. Salunkhe, N. Suzuki, Y. Yamauchi, K.-C. Ho, K.C.W. Wu, *Sci. Rep.*, 2014, **4**, 6983.
- 39 Q. Liu, Z.-X. Low, Y. Feng, S. Leong, Z. Zhong, J. Yao, K. Hapgood, H. Wang, *Microporous Mesoporous Mater.*, 2014, **194**, 1-7.
- 40 Y. Li, Z. Che, X. Sun, J. Dou, M. Wei, *Chem. Commun.*, 2014, **50**, 9769-9772.
- 41 Z. Wang, X. Li, H. Xu, Y. Yang, Y. Cui, H. Pan, Z. Wang, B. Chen, G. Qian, *J. Mater. Chem. A*, 2014, **2**, 12571-12575.
- 42 S.H. Ahn, W.S. Chi, D.J. Kim, S.Y. Heo, J.H. Kim, *Adv. Funct. Mater.*, 2013, **23**, 3901-3908.
- 43 D.K. Roh, W.S. Chi, H. Jeon, S.J. Kim, J.H. Kim, *Adv. Funct. Mater.*, 2014, **24**, 379-386.
- 44 S.H. Ahn, D.J. Kim, W.S. Chi, J.H. Kim, *Adv. Funct. Mater.*, 2014, **24**, 5037-5044.
- 45 D.J. Kim, J.K. Koh, C.S. Lee, J.H. Kim, *Adv. Energy Mater.*, 2014, **4**, 1400414.
- 46 M. Dan-Hardi, C. Serre, T. Frot, L. Rozes, G. Maurin, C. Sanchez, G. Férey, *J. Am. Chem. Soc.*, 2009, **131**, 10857-10859.
- 47 S. Hu, M. Liu, K. Li, Y. Zuo, A. Zhang, C. Song, G. Zhang, X. Guo, *CrystEngComm*, 2014, **16**, 9645-9650.
- 48 L. Shen, M. Luo, L. Huang, P. Feng, L. Wu, *Inorg. Chem.*, 2015, **54**, 1191-1196.
- 49 J. Yao, R. Chen, K. Wang, H. Wang, *Microporous Mesoporous Mater.*, 2013, **165**, 200-204.
- 50 I.D. Ivanchikova, J.S. Lee, N.V. Maksimchuk, A.N. Shmakov, Y.A. Chesalov, A.B. Ayupov, Y.K. Hwang, C.-H. Jun, J.-S. Chang, O.A. Kholdeeva, *Eur. J. Inorg. Chem.*, 2014, **2014**, 132-139.
- 51 Y. Wang, P. Sun, S. Cong, J. Zhao, G. Zou, *Carbon*, 2015, **92**, 262-270.
- 52 L. Tao, Z. Huo, Y. Ding, Y. Li, S. Dai, L. Wang, J. Zhu, X. Pan, B. Zhang, J. Yao, M.K. Nazeeruddin, M. Gratzel, *J. Mater. Chem. A*, 2015, **3**, 2344-2352.
- 53 X. Wang, R. Deng, S.A. Kulkarni, X. Wang, S.S. Pramana, C.C. Wong, M. Gratzel, S. Uchida, S.G. Mhaisalkar, *J. Mater. Chem. A*, 2013, **1**, 4345-4351.
- 54 D. J. Kim, S. H. Ahn, C. S. Lee, J. H. Kim, *J. Mater. Chem. A*, 2015, **3**, 17644-17651.
- 55 S. H. Ahn, D. J. Kim, W. S. Chi, J. H. Kim, *J. Mater. Chem. A*, 2015, **3**, 10439-10447.
- 56 F. Lodermeier, R. D. Costa, R. Casillas, F. T. U. Kohler, P. Wasserscheid, M. Prato and D. M. Guldi, *Energy Env. Sci*, 2015, **8**, 241-246.
- 57 H. Wang, J. Li, F. Gong, G. Zhou, and Z. S. Wang, *J. Am. Chem. Soc.*, 2013, **135**, 12627-12633.
- 58 C. Xu, J. Wu, U. V. Desai, D. Gao, *Nano Lett.* 2012, **12**, 2420-2424.
- 59 H. Wang, X. Zhang, F. Gong, G. Zhou, Z.-S. Wang, *Adv. Mater.* 2012, **24**, 121-124.
- 60 W. Zhang, J. Li, S. Jiang, Z. S. Wang, *Chem. Commun.* 2014, **50**, 1685-1687.

A shape- and morphology-controlled MIL-125(Ti) was synthesized using poly(ethylene glycol) diglycidyl ether (PEGDGE) as a structure directing agent. Upon deliberate calcination, MIL-125(Ti) was converted to mesoporous hierarchical TiO_2 (hier- TiO_2) with anatase phase and a large surface area. Dye-sensitized solar cell (DSSC) fabricated with the hier- TiO_2 photoanode and a solid electrolyte exhibited a high efficiency of 8.0%.

